Identification of systems containing nonlinear stiffnesses using backbone curves

Julián M. Londoño[a,*], Jonathan E. Cooper[b], Simon A. Neild[a]

[a] *Department of Mechanical Engineering, University of Bristol, Queens Building, University Walk, Bristol, BS8 1TR, UK*
[b] *Department of Aerospace Engineering, University of Bristol, Queens Building, University Walk, Bristol, BS8 1TR, UK*

Abstract

This paper presents a method for the dynamic identification of structures containing discrete nonlinear stiffnesses. The approach requires the structure to be excited at a single resonant frequency, enabling measurements to be made in regimes of large displacements where nonlinearities are more likely to be significant. Measured resonant decay data is used to estimate the system backbone curves. Linear natural frequencies and nonlinear parameters are identified using these backbone curves assuming a form for the nonlinear behaviour. Numerical and experimental examples, inspired by an aerospace industry test case study, are considered to illustrate how the method can be applied. Results from these models demonstrate that the method can successfully deliver nonlinear models able to predict the response of the test structure nonlinear dynamics.

Keywords: Nonlinear Identification, Nonlinear structural dynamics, Backbone curves, Resonance Decay Method

1. Introduction

With the continual drive for more efficient and lightweight structures, increasingly nonlinear structural dynamics are being observed in industrial

*Corresponding author
Email addresses: Julian.Londono@bristol.ac.uk (Julián M. Londoño), J.E.Cooper@bristol.ac.uk (Jonathan E. Cooper), Simon.Neild@bristol.ac.uk (Simon A. Neild)

applications. This presents a problem when developing accurate dynamic models of the structure as conventional parameter identification techniques almost always involves measurement of the modal parameters of the structure. This relies on the fundamental assumption of linearity and superposition, see for example [1]. For nonlinear systems, a range of identification techniques have been proposed, many of which are discussed in the overviews by Worden and Tomlinson [2] and Kerschen *et al.* [3]. Approaches that have been applied to multi-degree of freedom systems using forced response data include the restoring force method [4, 5], reverse path approaches [6] and NARMAX methods [7]. Bayesian fitting approaches are also being developed, although currently these mainly consider single degree-of-freedom systems [8, 9]. An alternative to forced response data is to measure the resonant decay; this is done by forcing the system onto a resonance and then letting the response decay as presented in [10]. Feldman also developed an estimation method for single-degree of freedom systems [11] which has been applied to multi-degree of freedom systems with non-proportional damping [12] and a system with a localised nonlinearity [13].

To better understand the nonlinear dynamics of a structure, Rosenberg [14] discussed the idea of the nonlinear normal mode (NNM) as an extension to linear modes for nonlinear systems. Such modes were defined as a vibration-in-unison of the unforced, undamped system with all the degrees-of-freedom passing through zero and reaching their extreme values in unison with each other. Due to nonlinearities, NNMs often vary both as a function of maximum amplitude of vibration and over each oscillation of a mode. Notable early contributions to the development of NNMs includes Rand [15] and Vakakis *et al.* [16]. In addition, Shaw and Pierre [17] considered the presence of damping on such modes. Recently, NNMs have more typically be thought of as a periodic response of the unforced, undamped system, allowing, for example, responses in anti-phase such as whirling of a cable to be treated as an NNM [18].

NNMs can be shown in the frequency-amplitude projection revealing the backbones of the system. If these are considered in the linear modal domain, then the interactions between the linear modes that make up the various NNM solutions are revealed [19]. If the nonlinearities are *smooth*, analytical expressions have been derived for NNMs using perturbation techniques. Using normal forms [20, 21], a state-space formulation for NNM responses has been reported [22, 23]. More recently a normal form method that is applied directly to the modal equations of motion, the second-order normal

forms [24, 25], has been used to examine NNMs in terms of the interactions between modes of the linearised structure [18, 19].

A methodology to extract the energy dependency of NNM modal curves and their frequencies from decaying time series is presented in [26]. It uses an extension of the force appropriation method [5] to nonlinear system and wavelet transform to perform the time-frequency analysis. This methodology to extract NNMs is later demonstrated experimentally in [27] using a cantilever beam with a geometric nonlinearity. They report the use of the conditioned reverse path method to identify the nonlinear behaviour of the beam. Following this, the identified model is used to produce theoretical NNMs which are compared to the experimentally measured NNMs.

Here we consider the use of experimentally measured resonant decay data, along with modal expressions for the equations of motion, as a mean to identify the nonlinear parameters in a system. Unlike the approach demonstrated in [26, 27], we use a methodology based on Moving Average filtering and zero-crossing detection to estimate the instantaneous frequency and amplitude of the decaying signal, thus extracting backbones curves in terms of amplitude-frequency maps as discussed in [28]. We use these amplitude-frequency relationships to identify nonlinear terms directly from the backbone curves since they can be more easily mapped onto stiffness nonlinearities. In this work, resonant decay data is taken from a nonlinear structure, a wing-nonlinear pylon inspired testpiece, and the experimental backbone curves of the test structure are estimated. Analytical expressions for the backbone curves are derived based on assumed nonlinear stiffness characteristics. These, together with the resonant decay data, are used to find suitable values for the nonlinear parameter in the model. The identification approach presented is applicable to lightly damped structural systems with smooth stiffness nonlinearities and resonant responses that are primarily dominated by their principal harmonic. This paper is organised as follows. Section 2 introduces the approach proposed in this work for the identification of structures containing elements with nonlinear stiffness. A simulated multi–degree–of–freedom (MDOF) system with two nonlinear elements is used in Section 3 to illustrate how the nonlinear parameters can be identified from the system backbone curves. The procedure is then applied to a nonlinear test structure in Section 4, closing with some final comments and remarks in the conclusions.

2. Identification of nonlinear parameters from experimental backbone curves

It is common for structures to be approximately linear at low vibration levels, but exhibit nonlinear behaviour as excitation levels increase. For this type of structure, the first task in system identification is to use conventional modal testing techniques, such as those described in [1], to identify the underlying linear system; that is, to estimate the linear mode shapes, natural frequencies and damping ratios within the frequency bandwidth of interest. Perhaps the fastest procedure consists of gently vibrating the test structure using broadband random excitation to measure the system's Frequency Response Functions (FRF), and from them, to determine the modal model of the underlying linear system. Following this linear identification, the contribution of the nonlinear elements can be investigated.

A useful tool capable of offering an understanding of the behaviour of nonlinear systems is the backbone curve [19]. These curves define natural frequencies as a function of response amplitude for a system when no damping or forcing is present. A technique for extracting backbones involves estimating both the instantaneous amplitude and frequency of the nonlinear system over its free vibration response. Note that as the system will inevitably have damping, the response is only a good approximation to its undamped backbone curve if the damping is reasonably light.

In this work we use the methodology presented in [28] to estimate the system backbones. In brief, it consists of applying a force pattern to the structure at the relevant frequency of interest using harmonic excitation. Once the structure is responding at the desired resonance condition, the input is removed and the response of the structure is free to decay from the steady–state resonant response. The resonance decay response is then mapped into the linear modal space and the instantaneous frequency and amplitude envelope in terms of each linear modal coordinate calculated. As in [28], here we use zero-crossings and peak amplitudes to calculate the instantaneous frequency and amplitude envelop over time respectively.

As long as the level of vibration in the steady–state is large enough to activate the structural nonlinearities, the estimated backbone curves can be used to find various nonlinear parameters able to model the system dynamics. We recall that other methods such as those presented in [11] and [27] could be used to estimate backbone curves provided that the frequency-amplitude dependency in terms of modal coordinates are given.

To develop the nonlinear model it is necessary to hypothesise a nonlinear stiffness function that captures the form of the nonlinearity. Hints on this might be drawn from the form of the estimated backbone curves or from static test data if available. Using this, the linear modal model can be extended by adding to each modal equation a trial nonlinear function that takes into account the modal interaction already revealed by the experimental backbone curves. As shown later with an example (see Section 3.2), this extended modal model can be reduced to a first order approximation in which only the dominant harmonic is kept. Here, we use the Harmonic Balance method to produce an analytic expression of the backbone curves based on the assumed nonlinear functions.

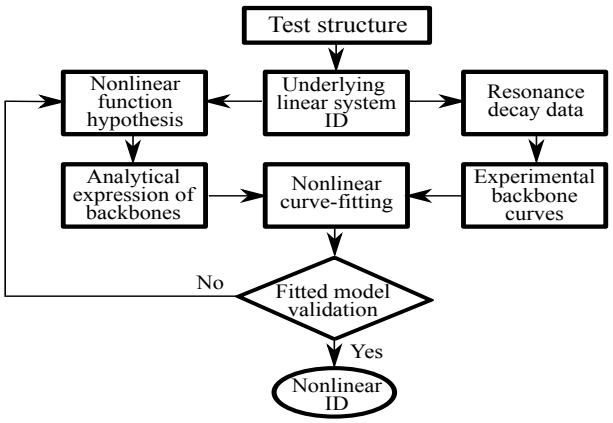

Figure 1: Diagram of the proposed procedure for the identification of nonlinear systems from backbone curves.

The approach proceeds by curve-fitting the analytical expressions of the backbones to the corresponding experimental curves for each resonance. This fitting allows for the nonlinear parameters present in the assumed model to be estimated. Ultimately, the performance of the fitted model can be assessed by predicting the system response at different levels of excitation and comparing the simulation results to the experimentally measured backbone curves. The diagram presented in Figure 1 summarises the procedure used here for the identification of the nonlinear system. The following sections illustrate the application of the proposed procedure on an aerospace inspired wing–pylon structure, firstly numerically and then experimentally.

3. Example of a nonlinear MDOF system

The example model studied here is a wing–pylon inspired structure. It consists of a continuous beam, the wing. Two masses, representing the stores, are suspended underneath beam and connected to it using nonlinear rotational springs that represent the pylons (as illustrated in Figure 2). The uniform beam is supported by two linear springs, of stiffness k=100N/m,attached to the ends of the beam. The forces generated by the nonlinear pylon springs are assumed to take the form

$$f_{s_i} = k_s\theta_i + k_2\theta_i|\theta_i| + k_3\theta_i^3 \tag{1}$$

where k_s=195Nm/rad; k_2=-1×10^5Nm/rad^2; k_3=1.36×10^9Nm/rad^3 and θ_i is the angle that the i-th mass support arm rotates with respect to the beam.

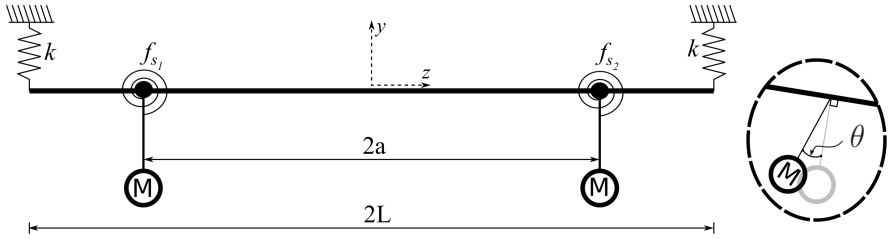

Figure 2: Example of a wing with stores on pylons connected through nonlinear rotational springs

Note that along with a positive cubic term producing hardening stiffness, we also consider a negative $\theta_i|\theta_i|$ nonlinear term, referred to as a quadratic term from now on, to produce a combined initial softening and then hardening stiffness as θ increases. The choice of $\theta_i|\theta_i|$ rather than θ_i^2 preserves the stiffness symmetry for positive and negative angles of rotation. The motivation for including this term is that it allows the backbone curve to have a non-infinite gradient on zero amplitude of response (see Appendix A) as is observed later in the experimental study. The equation of motion for the example structure is derived using the Lagrange method. The vertical deflection of the beam, y, is modelled such that

$$y(t,z) = \sum_{n=0}^{5} q_n(t)\left(\frac{z}{L}\right)^n; \qquad -L \le z \le L \tag{2}$$

This allows for two rigid-body modes and four flexural vibration modes. We consider an aluminium beam that is 1m long, 220mm wide and 5mm thick

with a density of 2700kg/m^3 and a Young's modulus of 70GPa. The store masses are 1.38Kg each and are located 200mm from the ends of the beam and suspended 100mm beneath it. Two lumped masses of 0.51Kg are also included on the beam to account for the mass of the pylon attachments.

Lagrangian mechanics was used to derive the mass and stiffness matrices for the equation of motion of the dynamical system, which can be written

$$\mathbf{M}\ddot{\mathbf{q}} + \mathbf{C}\dot{\mathbf{q}} + \mathbf{K}\mathbf{q} + k_3 \sum_{i=1}^{2} \rho_i^T (\rho_i \mathbf{q})^3 + k_2 \sum_{i=1}^{2} \rho_i^T |\rho_i \mathbf{q}| (\rho_i \mathbf{q}) = \mathbf{F} \tag{3}$$

The matrices of mass $\mathbf{M}$, damping $\mathbf{C}$ and stiffness $\mathbf{K}$, as well as the force vector $\mathbf{F}$, are presented in the Appendix B. We note that $\mathbf{C}$ is computed assuming a modal damping ratio of 0.5% for each linear mode. In this equation $\mathbf{q} = \{q_0,\ q_1,\ q_2,\ q_3,\ q_4,\ q_5,\ \theta_1,\ \theta_2\}^T$ and ρ is a location vector of the nonlinearities defined here as $\rho_1 = \{0,\ 0,\ 0,\ 0,\ 0,\ 0,\ 1,\ 0\}$ for the nonlinear spring on the left and $\rho_2 = \{0,\ 0,\ 0,\ 0,\ 0,\ 0,\ 0,\ 1\}$ for the other nonlinear spring. The linear pylon rotation stiffness terms, k_s, are included in the stiffness matrix $\mathbf{K}$.

The equations of motion for the system shown in Figure 2 can be transformed into linear modal space using the matrix of linear mode shapes Φ. Thus, the system dynamics can be expressed in term of the linear modal coordinates $\mathbf{u}(t)$ as in Equation (4), where the diagonal modal matrices for mass, damping and stiffness are: $\mathbf{M}_s = \Phi^T \mathbf{M} \Phi$; $\mathbf{C}_s = \Phi^T \mathbf{C} \Phi$ and $\mathbf{K}_s = \Phi^T \mathbf{K} \Phi$, giving

$$\mathbf{M}_s\ddot{\mathbf{u}} + \mathbf{C}_s\dot{\mathbf{u}} + \mathbf{K}_s\mathbf{u} + k_3 \sum_{i=1}^{2} \Phi^T \rho_i^T (\rho_i \Phi \mathbf{u})^3 + k_2 \sum_{i=1}^{2} \Phi^T \rho_i^T |\rho_i \Phi \mathbf{u}| (\rho_i \Phi \mathbf{u}) = \Phi^T \mathbf{F} \tag{4}$$

Here, $\mathbf{u} = \{u_{r_1},\ u_{r_2},\ u_1,\ u_2,\ u_3,\ u_4,\ u_5,\ u_6\}^T$, where u_{r_1} and u_{r_2} are the two rigid body modes and u_j is the j-th flexural vibration mode.

This study will be focused on the first four flexural modes of the underlying linear system named ϕ_1 to ϕ_4. Their natural frequencies and mode shapes are presented in Table 1 and shown in Figure 3. The complete matrix of mode shapes, that includes the rigid body modes, is presented in the Appendix C. We note that the modeshapes have been normalised with respect to the mass matrix $\mathbf{M}$.

	ϕ_1	ϕ_2	ϕ_3	ϕ_4
q_0	0.269	0.000	-0.688	0.000
q_1	-0.000	0.298	0.000	1.919
q_2	-0.862	-0.000	2.187	-0.000
q_3	0.000	-0.426	-0.000	-5.177
q_4	0.190	0.000	-0.458	-0.000
q_5	-0.000	0.165	0.000	1.785
θ_1	3.609	-5.475	6.546	5.453
θ_2	-3.609	-5.475	-6.546	5.453
$\xi_i(\%)$	0.5	0.5	0.5	0.5
f_n(Hz)	14.90	17.94	32.00	64.91

Table 1: Mode shapes, damping ratios and natural frequencies of the first four flexural modes of the underlying linear system for the nonlinear example

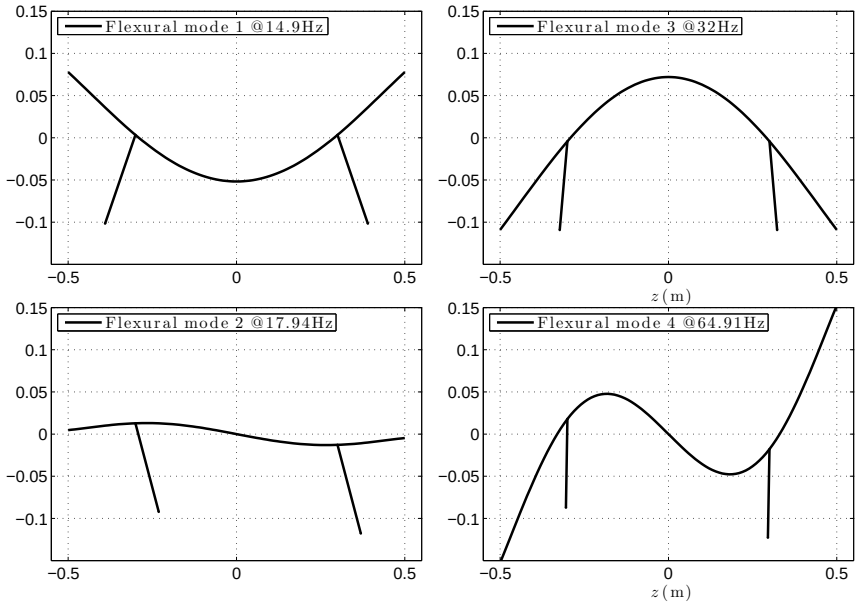

Figure 3: Schematics for the first four flexural mode shapes of the underlying linear dynamics of the example structure.

3.1. Simulated response of the dynamic model

To study the system dynamics, a vertical excitation is applied one-third of the way along the beam. Stepped sine responses at different levels of excita-

tion are simulated numerically for the system in Equation (3) over a range of frequencies around the linear natural frequencies presented in Table 1. These responses are mapped into the linear modal space and presented in Figure 4. Therein, U_i represents the spectral component of the i-th flexural vibration mode at the dominant frequency in the steady–state. Furthermore, using the procedure discussed in [28], and briefly introduced in Section 2, time-domain resonant decay simulations are carried out at each of the four resonances of interest. The resulting decays are used to estimate the backbone curves that characterise the response of the nonlinear structure. Due to the nonlinearity present in the structure, each resonance, while dominated by the linear mode close to the resonance, contains contributions from other modes. The backbone curves capture these linear modal contributions as a function of instantaneous frequency during the resonant decay. For both the analytical expression and the measured backbone curve, we calculate the resonant frequencies, so disregard contributions from higher modes in a consistent manner. The purpose of the numerical study is to assess the accuracy of the proposed identification procedure in which the correct solution is known. While the backbones could be computed directly for this numerical example, in general the nonlinearity is unknown and the backbone curves would be estimated from the system responses. Hence for consistency with Section 4, here we proceed as if the nonlinearity was unknown.

Figure 4 also presents the backbone curves estimated using resonant decay data (in dot-dashed red line). The first observation is that the backbone curves closely follow the peaks of the stepped responses and exhibit the same trend in terms of modal contributions at each resonance frequency. This indicates that the estimated backbone curves capture the nonlinear frequency–amplitude dependency of the structural response. Notice the non-infinite gradient of the backbone curves at zero amplitude and the initial softening which are produced by the quadratic stiffness term, with the subsequent hardening due to the influence of the cubic term of the nonlinear springs. This behaviour is also observed in the forced responses.

The first resonant response shows a significant contribution from the first mode to the system response. In addition, a contribution from the third linear mode is observed, but the contributions from the other linear modes is insignificant. In a similar way, the system response at the third resonance reveals a comparable behaviour with significant contribution from the third mode, a minor contribution from the first mode and negligible contributions from the other modes. This indicates a nonlinear coupling between modes 1

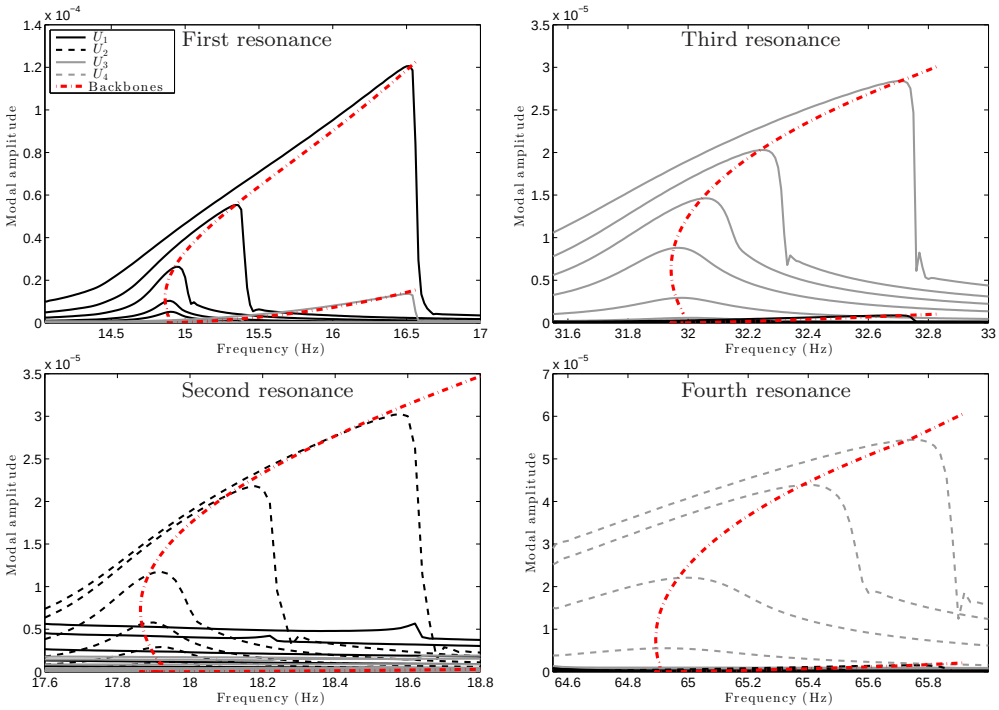

Figure 4: Backbone curves overlying the stepped sine responses of the example model around the four frequencies of interest. Here U_i is the spectral component of the i-th flexural vibration mode at each frequency in the steady–state.

and 3 that is evidenced in both the stepped sine responses and the estimated backbone curves.

A similar discussion can be made when considering the system response over the second and fourth resonance frequency bandwidths in Figure 4. The figure shows a weak nonlinear coupling between modes 2 and 4 without significant contribution from the other modes. However in addition to this, the plot for the second resonance shows a sustained contribution of mode 1 over the whole range of frequencies considered. This near constant action, rather than implying a significant modal coupling due to the nonlinearity, suggests that the second resonance was not isolated exactly using the single excitation point. The use of modal appropriation techniques, such as those described in [5], might be required to more exactly isolate the second resonance if cleaner stepped sine responses are needed. However, this approach falls beyond the scope of the present work.

3.2. Fitting a model from the backbone curves

Since we are interested in identifying the nonlinear stiffnesses using backbone curve measurements, we consider how the system in (4) behaves at resonance. Hence, considering only the first four flexural modes and following the observations above, we consider here the interaction between the symmetric flexural modes 1⇌3 and between the antisymmetric flexural modes 2⇌4. In doing this, we are able to reduce the nonlinear terms such that, for instance, row 3 and 5 of Equation (4) contain nonlinear terms with contribution from the flexural modes 1 and 3 only, assuming that the response for flexural modes 2 and 4 are insignificant when the resonant backbone curves dominated by flexural modes 1 or 3 are being considered.

To derive expressions for the backbone curves at the resonances in Table 1, we write a reduced modal equation from (4) and assume the system to be harmonically excited and vibrating at a resonance condition to get

$$\begin{aligned}
\ddot{u}_1 + 2\xi_1\omega_{n_1}\dot{u}_1 + \omega_{n_1}^2 u_1 + f_{nl_1}(u_1, u_3) &= f_1 \\
\ddot{u}_2 + 2\xi_2\omega_{n_2}\dot{u}_1 + \omega_{n_2}^2 u_2 + f_{nl_2}(u_2, u_4) &= f_2 \\
\ddot{u}_3 + 2\xi_3\omega_{n_3}\dot{u}_1 + \omega_{n_3}^2 u_3 + f_{nl_3}(u_1, u_3) &= f_3 \\
\ddot{u}_4 + 2\xi_4\omega_{n_4}\dot{u}_1 + \omega_{n_4}^2 u_4 + f_{nl_4}(u_2, u_4) &= f_4
\end{aligned} \tag{5}$$

Here, ω_{n_i} is the i-th natural frequency of the underlying linear system, ξ_i the damping ratio and f_{nl_i} is a nonlinear function of the interacting modal coordinates at the i-th resonance.

The Harmonic Balance (HB) method is used to find a first-order approximation of the above set of equations in which the higher harmonics terms are neglected. It assumes that the response of the system to a sinusoidal excitation is a sinusoid at the same frequency. The HB technique proceeds by substituting the excitations $f_i = A_i \sin(\omega t)$ and trial solutions $u_i = U_i \sin(\omega t + \psi_i)\ \forall i \in [1, 4]$, into Equation (5). Here A_i is the amplitude of the harmonic excitation and U_i represents the spectral component of the i-th mode at the dominant frequency in the steady–state. Thus, after a lengthy but straightforward calculation, the fundamental components can be extracted and simplified leading to an analytical expression of the backbone curves, such that

$$-\omega^2 U_i + \omega_{n_i}^2 U_i + \tilde{f}_{nl_i} = 0 \tag{6}$$

where $\tilde{f}_{nl_i}$ is the harmonic component within the i-th nonlinear function f_{nl_i}. Assuming the nonlinearity to be polynomial of the form $f_{nl_i} = a_i(c_j U_j + c_k U_k)|(c_j U_j + c_k U_k)| + b_i(c_j U_j + c_k U_k)^3 + d_i(c_j U_j + c_k U_k)^5$, where a_i, b_i, c_i and

d_i are arbitrary parameters of the i-th nonlinear function and the interacting modes j and k, and using harmonic balance, $\tilde{f}_{nl_i}$ may be written in the general form

$$\begin{aligned}
\tilde{f}_{nl_1} &= \tfrac{8}{3\pi}a_1(V_{13})|V_{13}| + \tfrac{3}{4}b_1(V_{13})^3 + \tfrac{5}{8}d_1(V_{13})^5, \\
\tilde{f}_{nl_2} &= \tfrac{8}{3\pi}a_2(V_{24})|V_{24}| + \tfrac{3}{4}b_2(V_{24})^3 + \tfrac{5}{8}d_2(V_{24})^5, \\
\tilde{f}_{nl_3} &= \tfrac{8}{3\pi}a_3(V_{13})|V_{13}| + \tfrac{3}{4}b_3(V_{13})^3 + \tfrac{5}{8}d_3(V_{13})^5, \\
\tilde{f}_{nl_4} &= \tfrac{8}{3\pi}a_4(V_{24})|V_{24}| + \tfrac{3}{4}b_4(V_{24})^3 + \tfrac{5}{8}d_4(V_{24})^5.
\end{aligned} \tag{7}$$

where $V_{13} = (c_1U_1 + c_3U_3)$, $V_{24} = (c_2U_2 + c_4U_4)$, and the first, second and third terms on the right hand side of these equations correspond to the quadratic, cubic and quintic nonlinearities respectively. We note that higher-order polynomials might be needed to fit more general nonlinearities.

Equation (6) can directly be correlated with the backbone curves previously estimated from the decay responses of the system (Figure 4). Hence for instance, using the sets of backbone curves corresponding to U_1 and U_3 over the frequencies of the first and third resonances, the unknown coefficients a_1, a_3, b_1, b_3, c_1, c_3, d_1 and d_3 can be estimated by simultaneously curve–fitting both the first and third equations of the assumed model to these data. Similarly, the second and fourth equations of the selected set can be curve–fitted to the backbone curves corresponding to U_2 and U_4 for the second and fourth resonances. Since the backbone curves are defined as a function of ω-U_i, the curve-fitting can be setup in such a way that the natural frequencies ω_{n_i} of the identified underlying linear system can either be used or be left as unknown parameters to be fitted. A statistical measure of goodness of fit could be used to make a decision on the setting that delivers the more accurate solution.

Considering three models, cubic only, cubic+quintic and quadratic+cubic, Table 2 presents the resulting coefficients of the best fitting cases, using nonlinear least squares fitting, for the first couple of interacting modes 1 and 3. In addition, the true values of the coefficients are given. In a similar way, the goodness of fit can be assessed in Figure 5, where the output of the best fitting case for the three trial models have been plotted on top of the measured backbone curves. It is worth noting that only the nonlinear model which includes the quadratic term is able to capture the softening behaviour at small displacements. Furthermore, note that the coefficients of the best fitting case of the latest nonlinear model are very close to the true values. To assess the impact of these differences, the fitted models are tested regard-

Nonlinear model		True coefficients	Cubic	Cubic+ quintic	Quadratic +cubic
Coeffs. of best fitting case	a_1 ($\times 10^7$)	-3.09	–	–	-3.19
	a_3 ($\times 10^7$)	-5.61	–	–	-5.68
	b_1 ($\times 10^{12}$)	2.75	1.84	1.54	2.83
	b_3 ($\times 10^{12}$)	5.00	3.09	2.76	5.05
	c_1	0.551	0.594	0.558	0.562
	c_3	1.00	1.00	1.00	1.00
	d_1 ($\times 10^{20}$)	–	–	3.71	–
	d_3 ($\times 10^{20}$)	–	–	6.65	–
	$\hat{f}_1$ (Hz)	14.90	14.76	14.82	14.9 *(fixed)*
	$\hat{f}_3$ (Hz)	32.00	31.87	31.89	32.0 *(fixed)*

Table 2: Coefficients that fits the backbone curves in terms of U_1 and U_3 for the first and third resonances using Equation (6).

ing their ability to predict the actual system response given by Equation (3) in the next section. In addition, we note that better solutions were found when the system's natural frequencies were treated as free parameters for the cases of the cubic and cubic+quintic nonlinear functions. However for the quadratic+cubic case, using the natural frequencies identified via linear techniques resulted in the better fit. The best fit in each case is shown in Figure 5.

Nonlinear model		True coefficients	Cubic	Cubic+ quintic	Quadratic +cubic
Coeffs. of best fitting case	a_2 ($\times 10^7$)	3.26	–	–	3.06
	a_4 ($\times 10^7$)	-3.24	–	–	-3.04
	b_2 ($\times 10^{12}$)	-2.41	-1.81	-1.47	-2.38
	b_4 ($\times 10^{12}$)	2.40	1.82	1.46	2.37
	c_2	-1.004	-0.992	-1.009	-1.007
	c_4	1.00	1.00	1.00	1.00
	d_2 ($\times 10^{20}$)	–	–	-1.56	–
	d_4 ($\times 10^{20}$)	–	–	1.54	–
	$\hat{f}_2$ (Hz)	17.94	17.72	17.78	17.94 *(fixed)*
	$\hat{f}_4$ (Hz)	64.91	64.85	64.87	64.91 *(fixed)*

Table 3: Coefficients that fits the backbone curves in terms of U_2 and U_4 for the second and fourth resonances using Equation (6).

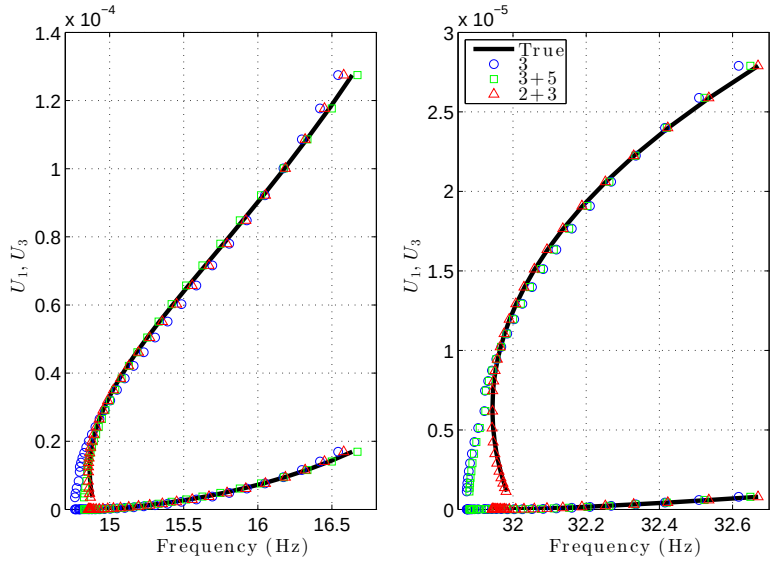

Figure 5: Best fitting case of the trial nonlinear models on top of the systems backbone curves for the first and third resonances.

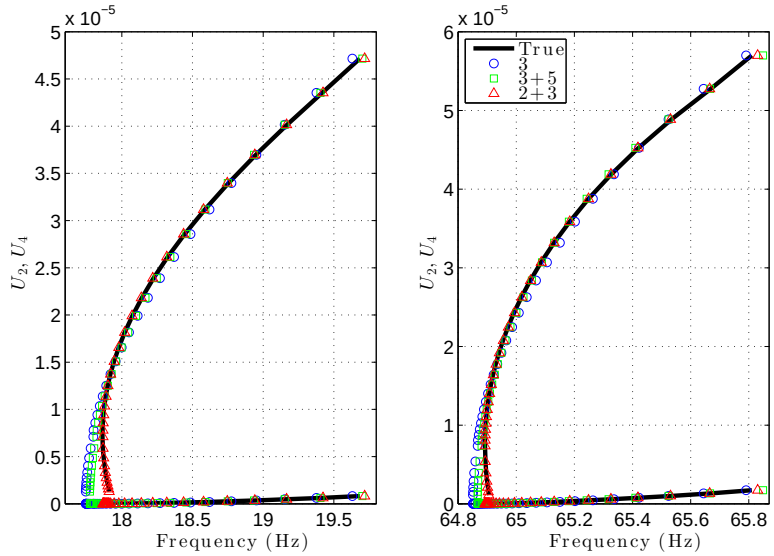

Figure 6: Best fitting case of the trial nonlinear models on top of the systems backbone curves for the second and fourth resonances.

Similarly, the backbone curves in terms of the modal amplitudes U_2 and U_4 corresponding to the second and fourth resonance frequencies were curve–

fitted to the second and fourth equations of the set in Equation (6), in accordance with the trial solution assumed. Table 3 presents the resulting coefficients of the best fitting cases for each trial solution. As before, the output of the best fitting cases for the three trial nonlinear models have been plotted on top of the backbone curves in Figure 6. Once again the coefficients of the nonlinear model that considers quadratic+cubic terms are very close to the true values.

3.3. Assessment of the fitted models

In order to verify the ability of the fitted nonlinear models in predicting the response of the actual system, sine stepped simulations have been conducted using the model given in Equation (4).

The top panels in Figure 7 presents the simulations around the first and third resonances of the fitted model that considers only cubic terms. In this and subsequent figures, the responses of the fitted models are plotted in solid black lines whereas the responses of the true model in Equation (4) are plotted in grey lines. The measured backbone curves have also been included to allow for further assessments. The fitted model is able to predict the system response, with best accurate within the mid-range of displacements. Since the cubic fitting could not model the initial softening behaviour, the prediction at small displacements is inaccurate and the resonance is missed. The bottom panel presents the simulations around the second and fourth resonance frequencies of the best fitting case for cubic nonlinearity. Here, it is much more evident that the assumed model is not able to reproduce the initial softening behaviour at low amplitudes. There is also a significant difference between the predicted and true responses for the highest level of forcing around the second resonance. This will be discussed in more detail shortly.

Figure 8 presents the response of the fitted model that considers the correct form of the nonlinearities with contributions of quadratic and cubic terms. This fitted model is able to predict accurately the responses of the example structure, with the best accuracy at small and medium level of displacements. Some differences can still be observed at large amplitudes for the first and third resonances. This is probably due to the fact that higher-order harmonics, which are ignored in the fitting process, affect the system response more significantly at these larger displacements. Nevertheless, the prediction is acceptable and arguably reflects the actual system behaviour within the range of amplitudes and frequencies presented. We note that

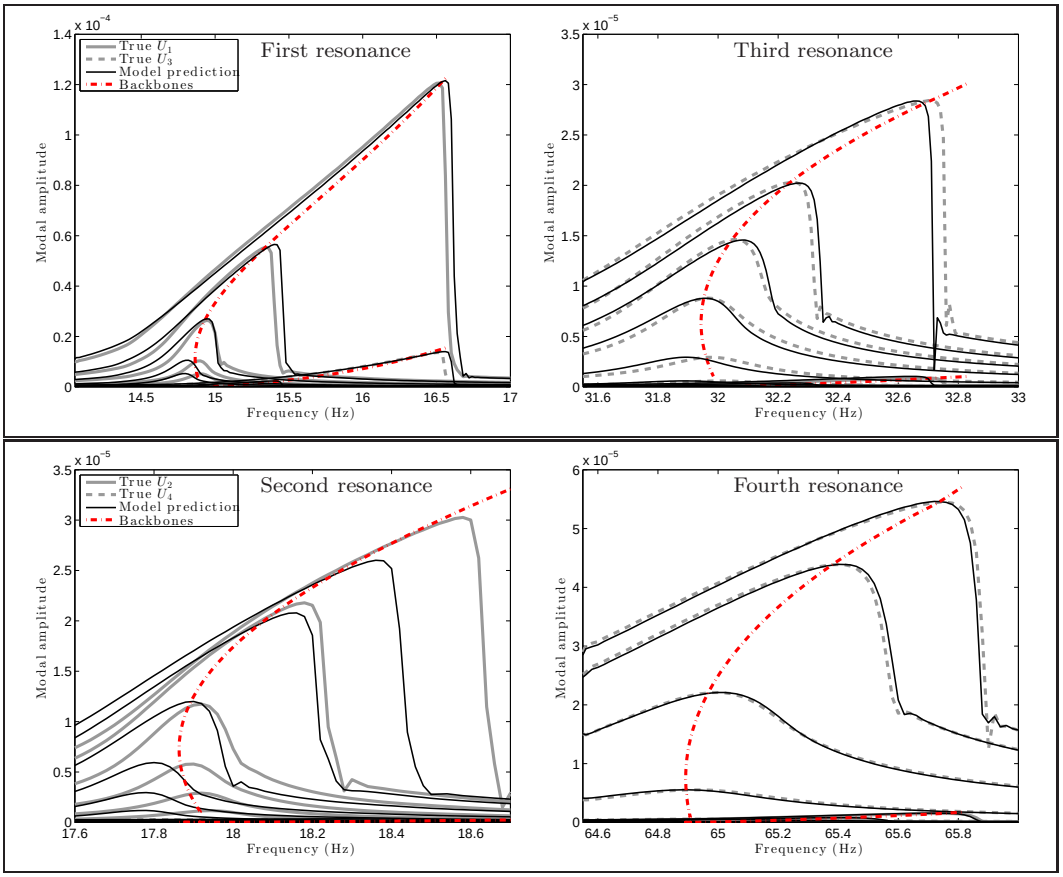

Figure 7: Sine stepped simulations of the fitted model that considers cubic nonlinearities only on top of the actual system response.

the use of more advances techniques such as the second–order normal forms method [25] that can accommodate the effects of higher harmonics may be of interest for improving this issue.

A notable difference can only be seen in the bottom-left panel of Figures 7 and 8 corresponding to the second resonance; where despite of the fact the response of fitted model follows the backbone curve, it underestimate the response of the actual system at larger amplitudes. This mismatch is a consequence of only considering the interaction of the antisymmetric flexural modes 2 and 4 when modelling the system at its second resonance. In doing this the effects of having two close modes (the first and the second modes), as can be observed in a linear system, are disregarded. Here for instance, the

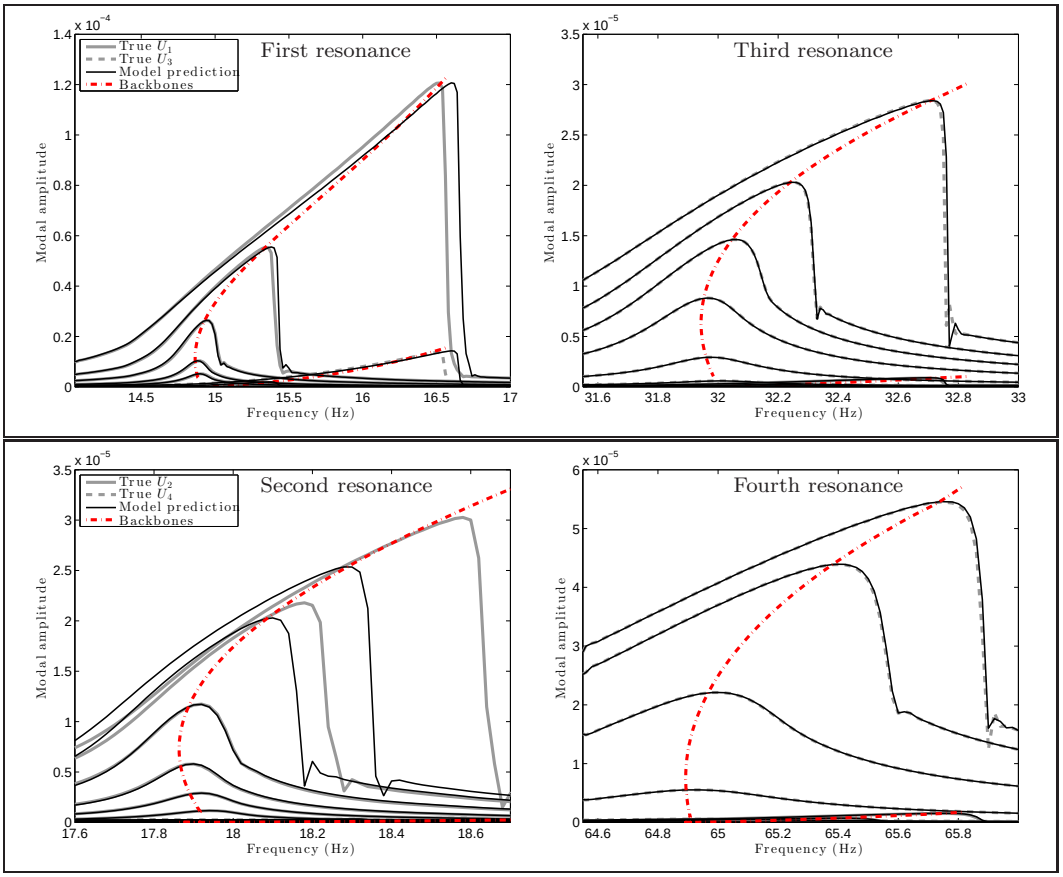

Figure 8: Sine stepped simulation of the fitted model that considers quadratic and cubic nonlinearities on top of the actual system response.

linear influence from the first linear mode onto the system's response at the second resonance was neglected in the set of equations (5). This interaction was also exhibited when estimating the backbone curves for the decay data from the second resonance; where the backbone curve measurement contained multiple non-harmonic frequencies. That is, the measured response contained a component of U_1, that was dominated by its own first resonant frequency, alongside the responses in U_2 and U_4, that were dominated by the excited second resonance frequency. The inclusion of this type of phenomena still remains an open research topic that falls outside the scope of this paper. Nevertheless, to assess the impact of this omission in the ability of the fitted model to predict the response of the example structure, we compare time-

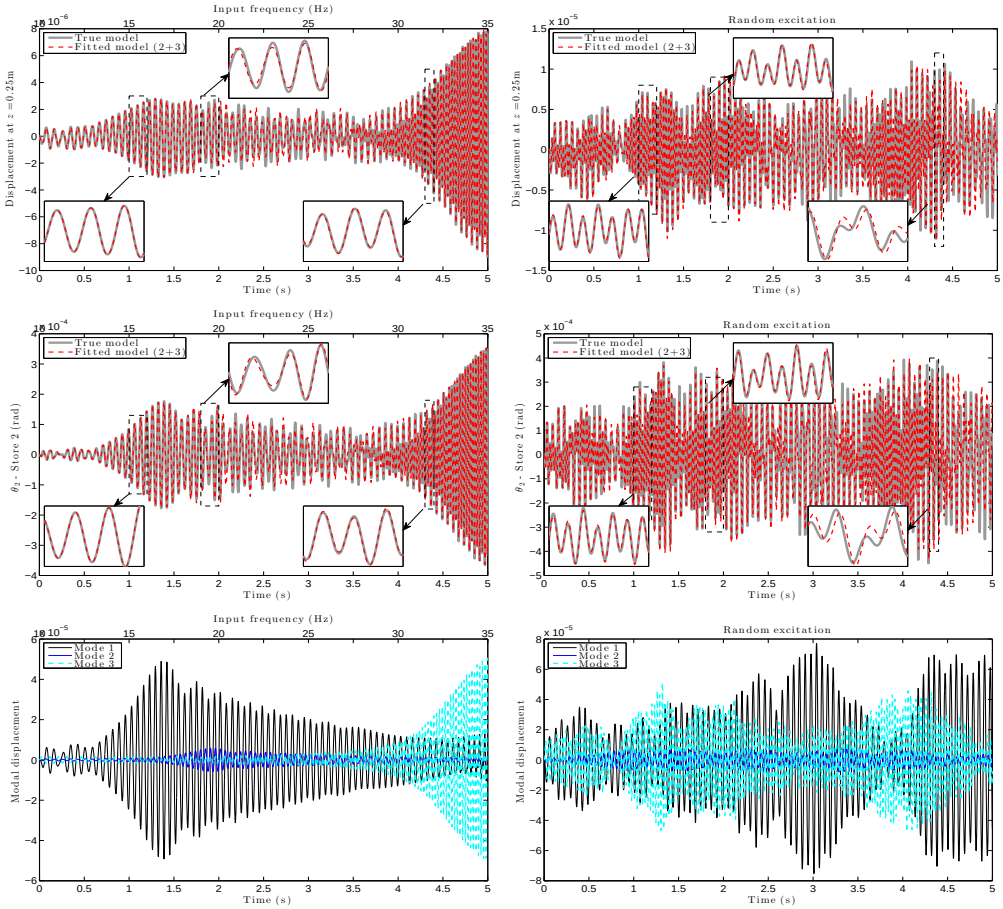

Figure 9: Vertical displacements of the beam at $z = 0.25$m (top panels), rotation of one pylon (middle panels) and modal displacements (lower panels) when simulating the response to a sine sweep (left-hand panels) and random (right-hand panels) excitation of the fitted model that considers quadratic and cubic nonlinearities on top of the responses of the true model of the example structure.

domain simulations of both models: the true model in Equation (3) and the fitted model that considers the nonlinear function with quadratic and cubic terms.

The left-hand side panels in Figure 9 present the responses to a sine sweep excitation covering the first three resonance frequencies (10Hz to 35Hz). The x-axis at the top of each panel displays the instantaneous excitation frequency along the simulation. The top panels correspond to the vertical displacement

at a quarter span, the middle panel shows the rotation of one of the stores and the lower panels present the results in terms of modal displacements. The zoomed windows present a close up of the responses that nearby the first, second and third resonance frequencies. It can be observed that the prediction of the fitted model is very accurate around the first and third resonances where the all the fundamental interactions where accounted for. However, in the vicinity of the second resonance frequency the fitted model cannot reproduce precisely the true response of the system. It is thought that this discrepancy is due to the exclusion of the linear influence of the first mode around the second resonance. Although not shown, the response near the fourth resonance is very good. The modal displacements shown in the lower panels of Figure 9 can be compared with those shown in Figure 8. We note that the excitation was large enough to produce modal displacements in the nonlinear regime.

Responses to random excitation are shown in the right-hand side panels of Figure 9. The results show that the fitted model is able to predict the response of the true structural model with reasonable accuracy. Some differences can be seen after 3s in the simulation. This is due to the fact that the structural response reached displacements where the fitted model starts to losing validity, here the first mode response approaches a level corresponding to the highest amplitude response in Figure 8.

4. Experimental example

We now consider applying the same method to experimental data where the true dynamic behaviour is unknown. As with the structure used in the numerical study in the previous section, the test structure approximately represents the configuration of an aircraft wing having two underwing stores (e.g., engines) with nonlinear pylon connections. The model consists of a rectangular aluminium plate hung by elastic chords and two lumped masses suspended underneath via pylon plates, as shown in Figure 10.

The nonlinear connection is built by fixing the pylon plates onto the wing using two bespoke clamps. This connecting element features internal curve surfaces that produces nonlinear behaviour through shortening the effective length of the pylon as it deflects. This wing structure was previously tested in [29] using the Resonance Decay Method approach. The model is excited by an electrodynamic shaker (LDS V201) and instrumented with 9 piezoelectric accelerometers (PCB 33M07) and two force sensors (PCB 208C03)

to measure the shakers driving force. Additionally, a laser Doppler vibrometer (PDV-100) is used to measure the velocity in the horizontal direction for one of the stores. Laser readings are used only to verify the processed data after numerically integrating the acquired acceleration signals. The vibration tests were controlled and recorded using LMS SCADAS Lab.

A number of tests were performed to gain insights into the overall structural behaviour of the wing model. These were also beneficial in determining the frequency of vibration and mode shapes that could be significantly influenced by the nonlinearities. Several dynamic tests were also conducted at

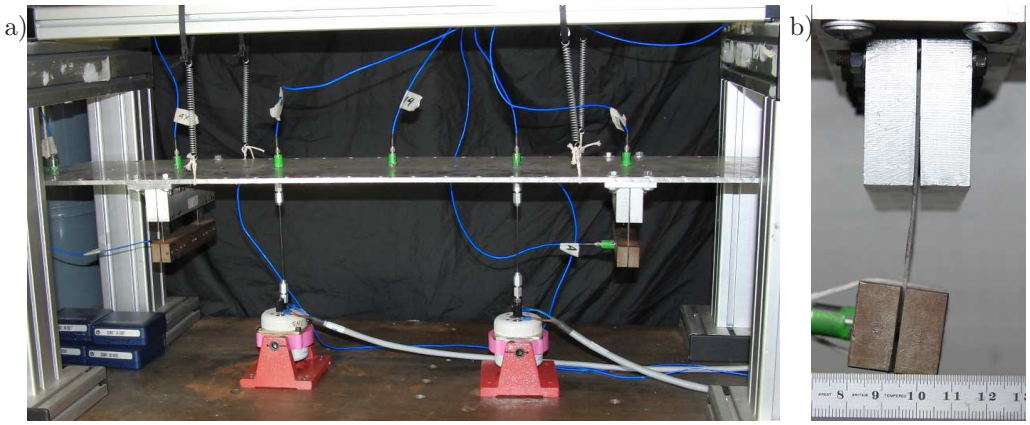

Figure 10: Test structure representing the configuration of an aircraft wing having two underwing stores supported by pylons. a) General view of the experimental setup. b) Close up of the nonlinear connection.

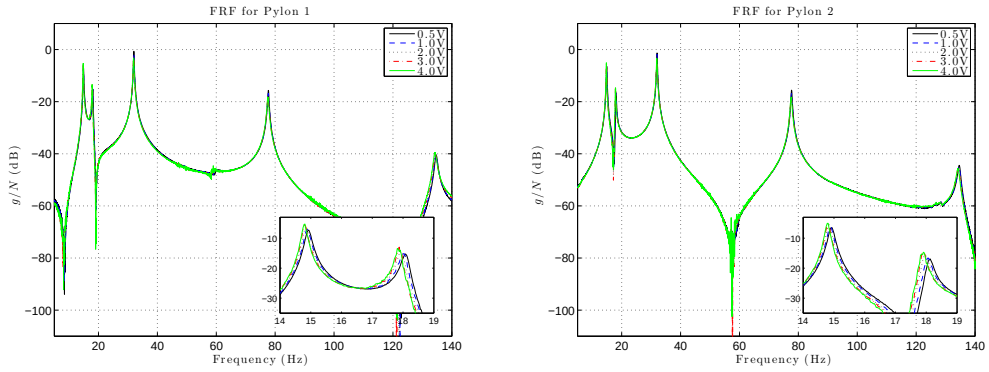

Figure 11: Set of FRFs for either pylon ends at different levels of vibration using random excitation. Note the softening effect exhibited by the resonance peaks in the zoomed boxes.

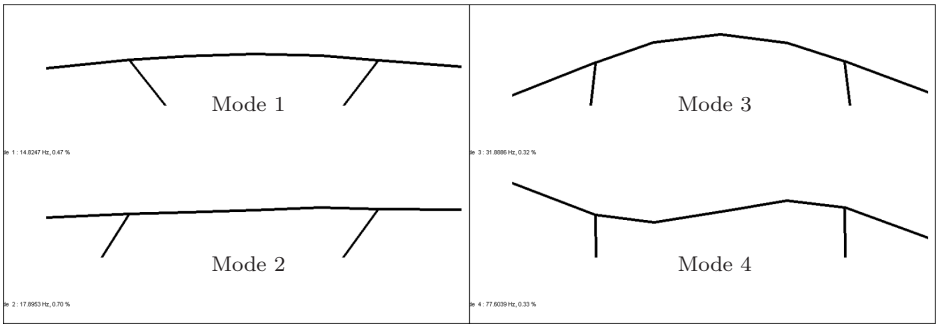

Figure 12: First four mode shapes of the underlying linear system of the test model.

different applied vibration levels. The driving force employed to vibrate the model were burst random signals with bandwidth of 256Hz on both shakers. Figure 11 presents FRFs measured at the end of either pylon for different increasing levels of excitation. In their estimation, 25 averages were used. It can be seen that the FRFs do not overlay each other for several modes indicating the presence of nonlinearities. Note that the zoomed plot within the figure reveals a clear softening effect. The frequency shift is mainly exhibited by the first two resonances located around 15Hz and 18Hz respectively. Also, we note that the maximum broadband random excitation using the shakers in Figure 10 can not produce motion on the stores large enough to reveal the full nonlinear behaviour, only the initial softening can be observed. Later stepped sine excitation is used to reveal hardening at higher amplitudes.

Classical modal testing [1] was used to obtain the shapes corresponding to the first four vibration modes, see Figure 12. The first and second modes describe the stores moving in anti–phase and in phase respectively. Whereas the third and fourth correspond to modes that are dominated by the first and second bending modes of the wing respectively, with reduced vibration of the stores. Therefore, the nonlinear behaviour is expected to mainly affect the structure when vibrating in either of the first two modes. So here, we discuss the dynamics associated with the first and second resonance frequencies and their interaction with other associated modes.

The first four mode shapes of the underlying linear system are presented in Table 4. The first seven rows correspond to the accelerometers located on the wing plate from left to right, and the last two rows, to the accelerometers located in the stores as shown in Figure 10. This matrix is used to operate a linear transformation on the decay records and thus obtain the structural

	ϕ_1	ϕ_2	ϕ_3	ϕ_4
z_1	-0.231	0.093	1.304	1.486
z_2	-0.014	0.079	0.098	-0.196
z_3	0.114	0.035	-0.628	-0.577
z_4	0.160	-0.009	-0.927	-0.003
z_5	0.105	-0.077	-0.621	0.587
z_6	-0.016	-0.069	0.063	0.218
z_7	-0.218	-0.042	1.185	-1.398
x_1	-1.114	-0.783	-0.170	-0.023
x_2	1.007	-0.983	0.183	-0.023
$\xi_i(\%)$	0.68	0.64	0.35	0.25
f_n(Hz)	14.91	18.09	32.01	77.69

Table 4: Mode shapes, damping ratios and natural frequencies of the underlying linear system for the test structure. The first seven rows correspond to vertical displacements along the wing plate (equally spaced) whereas the last two rows correspond to the radial displacement of the stores.

response in terms of the modal coordinates of the underlying linear system. The mode shapes reveal that the structure is not perfectly symmetric, which is probably due to differences in the linear stiffness characteristics of the pylons and subtle differences in their support conditions.

Following the procedure described in section 2 for the experimental estimation of backbone curves, sinusoidal excitation in force–control mode is applied to the test specimen at the desired near-resonant frequency using just a single shaker. The forcing frequency is gradually tuned until the amplitude of the response rises in magnitude and is large enough to activate the nonlinearity. When the system response reaches the state–steady condition, the shaker is turned off and the resonance decay recorded. The structural displacements are then calculated via double integration of the acceleration signals. These signals are mapped into the linear modal space using the matrix of mode shapes. Subsequently, the procedure for estimating the backbone curves is applied independently to each decaying response of the system expressed in terms of the linear modal coordinates. Because of the light damping, the number of oscillations over the decaying response is large enough to allow a good measure of the backbone curves. Note that since the shaker is still attached to the test specimen during the decay, its dynamics might have an impact on the resulting backbone curves. This effect,

which depends on the shaker characteristics and its attaching point to the structure, is being investigated and will be addressed in forthcoming work.

Figure 13a presents the resulting backbone curves estimated in terms of the modal amplitudes U_1, U_2, U_3 and U_4 from decaying signals corresponding to the first resonance frequency. The dominant backbone curve corresponds to the first modal amplitude U_1 (black solid line), as the structure was harmonically excited around the first resonant frequency. This curve clearly exhibits the initial softening behaviour already revealed by the random excitation tests, but also shows a stronger hardening behaviour at larger amplitudes as might be expected from the nonlinear connection shown in Figure 10b. Furthermore, it can be seen that when the structural response is large and the influence of the nonlinearity is much more significant, the modal contribution from U_2 and U_3 to the backbone curves start to increase. As before, this observation could be exploited by extending the modal equations to include coupled terms for nonlinear system identification purposes.

With the aim of verifying this modal interaction, Figure 13c presents the resulting backbone curves estimated from the decay response corresponding with the third resonance frequency. These results show a strong contribution to the structural responses in terms of the third modal coordinate U_3 (grey solid line) with some interaction from U_1 and U_2.

Similarly, the second and fourth resonance decays were recorded, mapped into the linear modal space and used to estimate the respective set of backbone curves. These are plotted in Figures 13b and 13d. The backbones for the second resonance exhibit some interaction from U_2, U_3 and U_4. With regards to the fourth resonance, it was not possible to excite the test structure sufficiently to obtain large store deflections even when the shaker was at its maximum capacity. No hardening behaviour is visible in these decay data. Hence, this paper will discuss only results based on the first and third interacting resonances.

4.1. Fitting a model from the backbone curves

Adopting the same approach as applied to the numerical system, we continue to assume that the system is symmetric. This assumption appears reasonable when inspecting the linear modeshapes in Figure 12, see also Table 4 where one can see that the error between symmetric locations is of the region of 5% for the first mode. In addition, this assumption allows the number of unknown terms to be kept low. As with the previous numerical

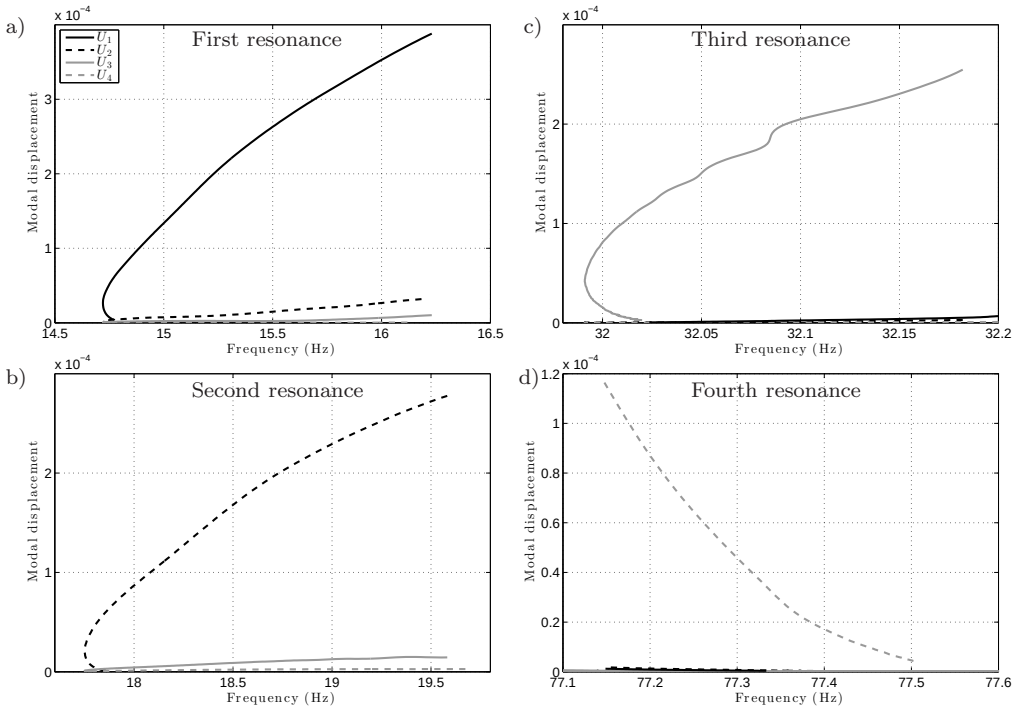

Figure 13: Backbone curves estimated from experimental data in terms of the modal coordinates U_1 to U_4

study, and due to the symmetry assumption, we consider the interaction between the symmetric modes 1⇌3 and the antisymmetric modes 2⇌4. The adequacy of this assumption will be discussed later when the ability of the fitted models to predict the system response are assessed. However we note that the first resonance, in contrast to the numerical system, exhibits some second linear modal content indicating a degree of asymmetry in the system. To account for this behaviour, we include in the fitting process the backbones curves in terms of the second linear modal coordinate as well as the equation corresponding to the second resonance. With this modification and considering two of the trial nonlinear functions used before, a cubic function and a cubic and quadratic function, the backbone curves are curve–fitted. This is done in terms of U_1, U_2 and U_3 over the range of frequencies corresponding to the first, second and third resonances simultaneously. Table 5 presents the results based on a nonlinear least squares optimisation procedure to find the best set of parameters for fitting the experimentally obtained backbone

curves with the selected set of equations. The backbone curves based on the fitted parameters are plotted alongside the experimental backbone curves in Figure 14. Here, unlike the numerical study, we do not know the cor-

Nonlinear model	Coefficients of the best fitting case								
	$a_1(\times 10^5)$	$a_2(\times 10^5)$	$a_3(\times 10^5)$	$b_1(\times 10^{10})$	$b_2(\times 10^{10})$	$b_3(\times 10^{10})$	c_1	c_2	c_3
Cubic	-	-	-	0.88	-4.76	0.19	1.00	-0.78	1.37
Quadratic+cubic	6.77	-1.20	0.49	0.63	-0.11	0.05	1.00	-2.58	1.99

Table 5: Coefficients that fit the experimental backbone curves in terms of U_1, U_2 and U_3 to the first, second and third resonances using Equation (6).

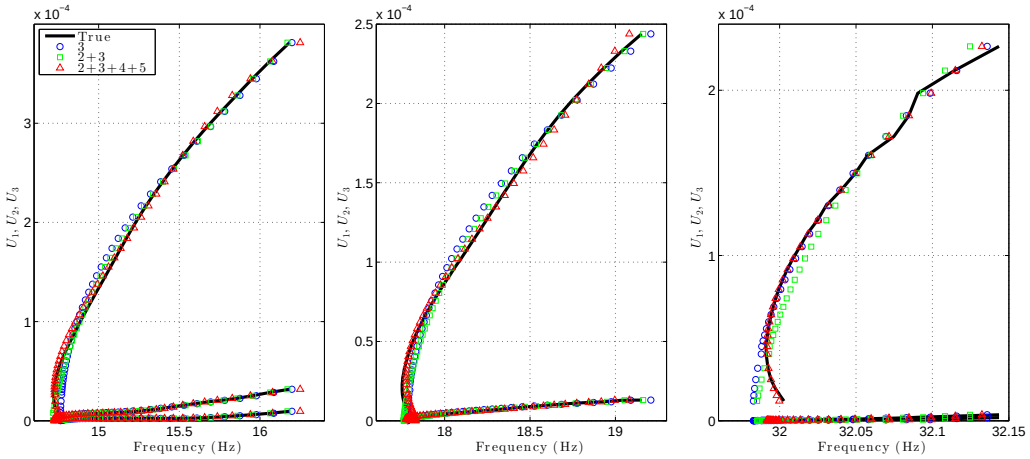

Figure 14: Best fitting case of the trial models on top of the experimental backbone curves.

rect parameter values. However it can be seen that neither of these nonlinear functions reproduces the rapid slope change of the initial softening behaviour exhibited in the measured backbone curves. A higher order polynomial that includes quadratic, cubic, quartic and quintic terms is used instead as a trial nonlinear function. This led to analytical expression for the backbone curves

given by

$$\begin{aligned} -\omega^2 U_1 + \omega_{n_1}^2 U_1 + \tfrac{8}{3\pi} a_1 V|V| + \tfrac{3}{4} b_1 V^3 + \tfrac{32}{15\pi} d_1 V^3|V| + \tfrac{5}{8} e_1 V^5 &= 0, \\ -\omega^2 U_2 + \omega_{n_2}^2 U_2 + \tfrac{8}{3\pi} a_2 V|V| + \tfrac{3}{4} b_2 V^3 + \tfrac{32}{15\pi} d_2 V^3|V| + \tfrac{5}{8} e_2 V^5 &= 0, \\ -\omega^2 U_3 + \omega_{n_3}^2 U_3 + \tfrac{8}{3\pi} a_3 V|V| + \tfrac{3}{4} b_3 V^3 + \tfrac{32}{15\pi} d_3 V^3|V| + \tfrac{5}{8} e_3 V^5 &= 0, \\ \text{where} \qquad V = (c_1 U_1 + c_2 U_3 + c_3 U_3). & \end{aligned} \tag{8}$$

The coefficients that best fit the experimental backbone curves to this set of equations are presented in Table 6 and the fitted model output plotted in Figure 14. It can be seen that this nonlinear function performs better in reproducing the experimentally observed features than the cubic or quadratic+cubic ones.

Nonlinear model	Coefficients of the best fitting case					
	i	a_i ($\times 10^6$)	b_i ($\times 10^{10}$)	c_i	d_i ($\times 10^{14}$)	e_i ($\times 10^{17}$)
Quadratic+ cubic+quartic+ quintic	1	−2.04	4.31	1.00	−1.64	2.31
	2	−3.18	6.72	1.16	−2.56	3.59
	3	−2.26	4.77	0.71	−1.82	2.55

Table 6: Coefficients that fit the experimental backbone curves in terms of U_1, U_2 and U_3 to the first, second and third resonances of the test structure using Equation (8).

4.2. Forced responses using the fitted models

Now we simulate the response of the fitted models with the purpose of assessing their ability to predict the response of the test structure. Sine stepped simulations at the increasing levels of excitations are computed at a range of frequencies around the first, second and third resonances. The responses of the fitted models are plotted in solid black lines and the experimental backbone are included in dashed red line to facilitate a direct comparison.

Figure 15 presents the simulation results of the fitted model that considers only cubic terms in the nonlinear functions. The peaks in the responses of the fitted model follow both experimental backbone curves U_1 and U_3 for both the first and third resonances. However, the fitted model fails to predict the contributions in terms of U_2 to the first resonance. Similarly, the peaks in the responses of the fitted model follow the experimental backbone curves U_2 for the second resonance but fail to predict the contribution in terms of U_3. This is due to the fact that we consider a symmetric model to fit the

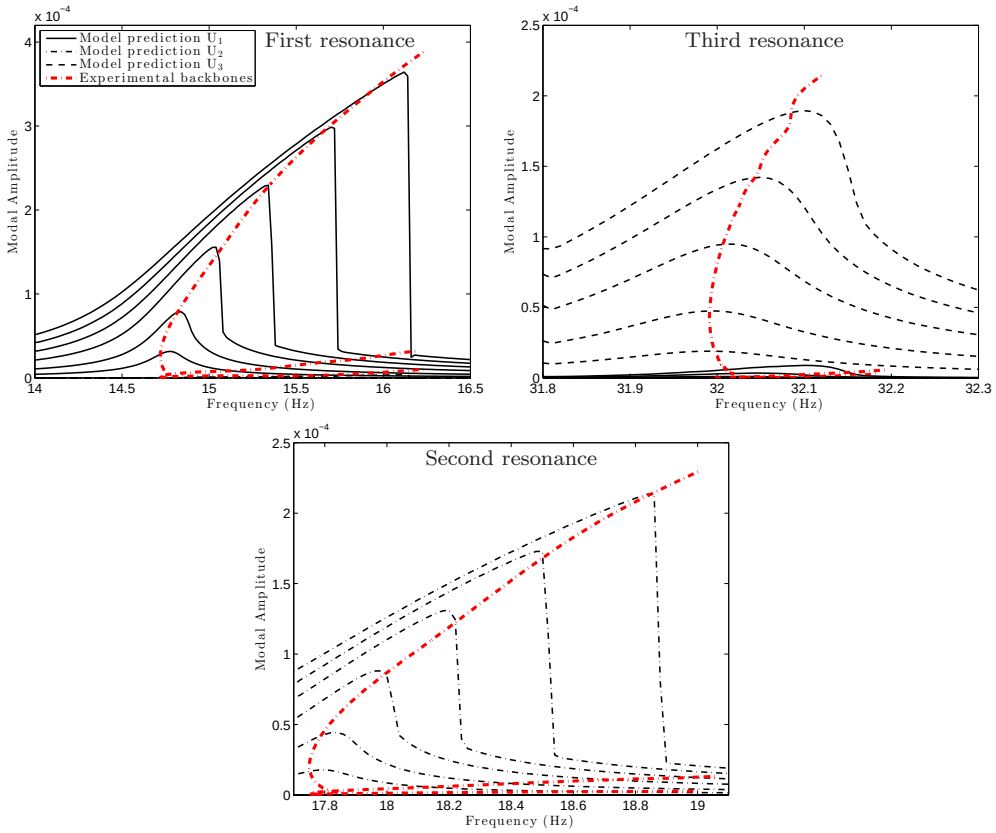

Figure 15: Sine stepped simulations of the fitted model that considers cubic nonlinearities only on top of the experimental backbone curves of the test structure.

backbone curves and so the interaction between symmetric and antisymmetric modes are not captured. In addition, since the cubic function could not fit the initial softening behaviour, the prediction at small displacements is not accurate. Figure 16 presents the stepped sine simulation of the fitted model that includes nonlinear functions with quadratic, cubic, quadric and quintic terms. Unlike the other two cases considered, the fitted model can reproduce the test structure's responses all over the range of displacements including being able to mimic the observed softening behaviour at small displacements. Note that the peaks of the stepped sine response coincide with the experimental backbone curves showing accuracy of the fitted model's prediction, but do not predict the contributions in terms of U_2 to the first resonance nor U_3 to the second resonance.

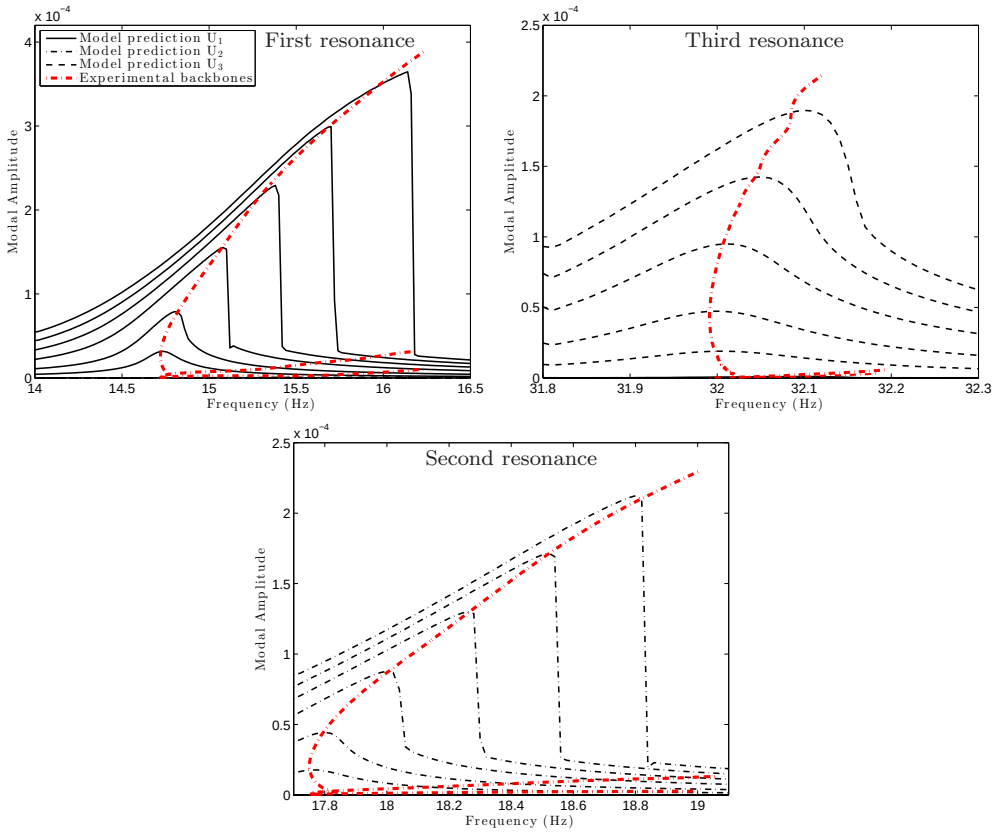

Figure 16: Sine stepped simulations of the fitted model that considers quadratic, cubic, quartic and quintic nonlinearities on top of the experimental backbone curves of the test structure.

5. Conclusions

This paper presents a method for the dynamic identification of structures containing discrete nonlinear stiffnesses based on experimental data. In contrast to methods that use random excitation for nonlinear system identification, the approach discussed here requires the structure to be excited at just a single resonant frequency, at any one time, enabling measurements to be made in larger displacement regimes where nonlinearities are more likely to be observed.

We have discussed the use of measured resonant decay data to estimate the system backbone curves. This data alongside modal equations of motion, that include nonlinear modal interaction terms, enables identification

of both linear frequencies and nonlinear parameters. Numerical and experimental examples inspired by an aerospace industry test case were considered to illustrate how the method can be applied. Results from these models demonstrate that the method can deliver nonlinear models able to predict the response of the test structure to a range of excitation within frequencies and amplitudes.

In the analytical example, which contains two discrete nonlinear elements with quadratic and cubic terms, we successfully identified the more significant nonlinear modal interaction terms between the first and third linear modes and between the second and fourth modes. In both cases the forced response using the fitted models accurately capture the interaction between the modes in question within the range of amplitudes and frequencies used in the fitting process. In addition, the fitted model accurately replicates the response due to stepped-sine excitation over the first, third and fourth resonances of the full system. However there are some discrepancies around the second resonance, which we believe is due to additional linear interactions with the first mode at this resonance, something that is currently unaccounted for in the fitting approach.

Experimental tests were conducted on a similar structure to the numerical one. Here we concentrated on the dynamics of the first mode and its interaction with the second and third. A symmetric model was fitted using the first, second and third resonant responses. Here as the form of the nonlinearity was unknown, several models were considered. It was found that to capture the curvature of the backbone curves at low as well as high response levels, polynomial terms up to fifth-order were needed. Also, results showed that the use of an asymmetric nonlinear model might be needed to accommodate the interaction of symmetric and antisymmetric modes. Nonetheless, this implies an increasing number of unknown variables to be fitted that might lead to a number of practical issues in the nonlinear curve–fitting process.

We also note that analytical expressions of the backbone curves based on assumed nonlinear characteristics are required in this approach. The success of this identification method depends upon the ability of the chosen nonlinear functions to reproduce the nonlinear characteristics revealed by the system's backbones. In this work we used polynomials in increasing order as the trial nonlinear functions. However, a more systematic way to choose suitable nonlinear functions remains an open research topic.

Acknowledgement

This work was funded by the Engineering and Physical Sciences Research Council (EPSRC) in the UK as part of the Engineering Nonlinearity Programme Grant EP/K003836/1. Prof. S. A. Neild is supported by the EPSRC Fellowship EP/K005375/1 and Prof. J. E. Cooper is supported by the Royal Academy of Engineering in the UK through the RAEng Airbus Sir George White Chair in Aerospace Engineering. This financial support is gratefully acknowledged.

References

[1] D. Ewins, Modal Testing: Theory, Practice and Application, 2nd Edition, Engineering Dynamics Series, Research Studies Press, Baldock, Hertfordshire, UK, 2000.

[2] K. Worden, G. Tomlinson, Nonlinearity in Structural Dynamics: Detection, Identification and Modelling, IOP Publishing Ltd, Bristol and Philadelphia, 2001.

[3] G. Kerschen, K. Worden, A. Vakakis, J.-C. Golinval, Past, present and future of nonlinear system identification in structural dynamics, Mechanical Systems and Signal Processing 20 (2006) 505–592. doi:10.1016/j.ymssp.2005.04.008.

[4] G. Kerschen, J.-C. Golinval, K. Worden, Theoretical and experimental identification of a non-linear beam, Journal of Sound and Vibration 244 (4) (2001) 597–613. doi:10.1006/jsvi.2000.3490.

[5] J. R. Wright, J. E. Cooper, M. J. Desforges, Normal–mode force appropriation – theory and application, Mechanical Systems and Signal Processing 13 (2) (1999) 217–240. doi:10.1006/mssp.1998.1214.

[6] G. Kerschen, J.-C. Golinval, Generation of accurate finite element models of nonlinear systems – application to an aeroplane-like structure, Nonlinear Dynamics 39 (1-2) (2005) 129–142. doi:10.1007/s11071-005-1919-8.

[7] S. Billings, Nonlinear System Identification: NARMAX Methods in the Time, Frequency and Spatio-Temporal Domains, Wiley, 2013.

[8] K. Worden, J. Hensman, Parameter estimation and model selection for a class of hysteretic systems using bayesian inference, Mechanical Systems and Signal Processing 32 (2012) 153–169, special Issue: Uncertainties in Structural Dynamics. doi:10.1016/j.ymssp.2012.03.019.

[9] P. Green, Bayesian system identification of a nonlinear dynamical system using a novel variant of simulated annealing, Mechanical Systems and Signal Processing 52–53 (2015) 133 –146. doi:dx.doi.org/10.1016/j.ymssp.2014.07.010.

[10] M. F. Platten, J. R. Wright, G. Dimitriadis, J. E. Cooper, Identification of multi–degree of freedom non–linear systems using an extended modal space model, Mechanical Systems and Signal Processing 23 (1) (2009) 8–29. doi:10.1016/j.ymssp.2007.11.016.

[11] M. Feldman, Non–linear system vibration analysis using Hilbert transform–I. Free vibration analysis method 'FREEVIB', Mechanical Systems and Signal Processing 8 (2) (1994) 119–127. doi:10.1006/mssp.1994.1011.

[12] S. Naylor, M. F. Platten, J. R. Wright, J. E. Cooper, Identification of multi–degree of freedom systems with nonproportional damping using the resonant decay method, J. Vib. Acoust 126 (2) (2004) 298–306. doi:10.1115/1.1687395.

[13] M. Feldman, Identification of weakly nonlinearities in multiple coupled oscillators, Journal of Sound and Vibration 303 (2) (2007) 357–370. doi:10.1016/j.jsv.2007.01.028.

[14] R. Rosenberg, The normal modes of nonlinear N-degree-of-freedom systems, Journal of Applied Mechanics 29 (1) (1962) 7–14. doi:10.1115/1.3636501.

[15] R. H. Rand, A direct method for non–linear normal modes, International Journal of Non-Linear Mechanics 9 (5) (1974) 363–368. doi:10.1016/0020-7462(74)90021-3.

[16] A. Vakakis, L. Manevitch, Y. Mikhlin, V. Pilipchuk, A. Zevin, Normal Modes and Localization in Nonlinear Systems, Wiley, New York, 1996. doi:10.1002/9783527617869.

[17] S. Shaw, C. Pierre, Normal modes for non–linear vibratory systems, Journal of Sound and Vibration 164 (1) (1993) 85–124. doi:10.1006/jsvi.1993.1198.

[18] T. L. Hill, A. Cammarano, S. A. Neild, D. J. Wagg, Out-of-unison resonance in weakly nonlinear coupled oscillators, Proceedings of the Royal Society of London A: Mathematical, Physical and Engineering Sciences 471 (2173). doi:10.1098/rspa.2014.0659.

[19] A. Cammarano, T. Hill, S. Neild, D. Wagg, Bifurcations of backbone curves for systems of coupled nonlinear two mass oscillator, Nonlinear Dynamics 77 (1-2) (2014) 311–320. doi:10.1007/s11071-014-1295-3.

[20] L. Jezequel, C. Lamarque, Analysis of non–linear dynamical systems by the normal form theory, Journal of Sound and Vibration 149 (3) (1991) 429–459. doi:10.1016/0022-460X(91)90446-Q.

[21] A. Nayfeh, Method of normal forms, Wiley, New York, 1993. doi:10.1002/9783527635801.

[22] A. H. Nayfeh, On direct methods for constructing nonlinear normal modes of continuous systems, Journal of Vibration and Control 1 (4) (1995) 389–430. doi:10.1177/107754639500100402.

[23] C. Touzé, O. Thomas, A. Huberdeau, Asymptotic non-linear normal modes for large-amplitude vibrations of continuous structures, Computers & Structures 82 (31–32) (2004) 2671–2682, nonlinear Dynamics of Continuous Systems. doi:10.1016/j.compstruc.2004.09.003.

[24] C. Touzé, O. Thomas, A. Chaigne, Hardening/softening behaviour in non-linear oscillations of structural systems using non-linear normal modes, Journal of Sound and Vibration 273 (1–2) (2004) 77–101. doi:10.1016/j.jsv.2003.04.005.

[25] S. A. Neild, D. J. Wagg, Applying the method of normal forms to second–order nonlinear vibration problems, Proceedings of the Royal Society of London A: Mathematical, Physical and Engineering Sciences 467 (2128) (2011) 1141–1163. doi:10.1098/rspa.2010.0270.

[26] M. Peeters, G. Kerschen, J. Golinval, Dynamic testing of nonlinear vibrating structures using nonlinear normal modes, Journal of Sound and Vibration 330 (3) (2011) 486 – 509. doi:10.1016/j.jsv.2010.08.028.

[27] M. Peeters, G. Kerschen, J. Golinval, Modal testing of nonlinear vibrating structures based on nonlinear normal modes: Experimental demonstration, Mechanical Systems and Signal Processing 25 (4) (2011) 1227–1247. doi:10.1016/j.ymssp.2010.11.006.

[28] J. M. Londoño, S. A. Neild, J. E. Cooper, Identification of backbone curves of nonlinear systems from resonance decay responses, Journal of Sound and Vibration 348 (2015) 224–238. doi:10.1016/j.jsv.2015.03.015.

[29] M. F. Platten, J. R. Wright, J. E. Cooper, G. Dimitriadis., Identification of a nonlinear wing structure using an extended modal model, Journal of Aircraft 46 (5) (2009) 1614–1626. doi:10.2514/1.42024.

Appendix A. Justification of the quadratic term

Consider the case of an undamped and unforced SDOF system with a quadratic nonlinearity of the form $u|u|$, or $u^2\text{sign}(u)$, such that

$$\ddot{u} + \omega_n^2 u + k u^2 \text{sign}(u) = 0 \tag{A.1}$$

We assume a periodic solution at resonance of the form $u(t) = U\cos(\omega t)$ and substitute it into the equation of motion to obtain

$$-\omega^2 U\cos(\omega t) + \omega_n^2 U\cos(\omega t) + \frac{1}{2}kU^2\left(1+\cos\left(2\omega t\right)\right)\text{sign}\left(\cos\left(\omega t\right)\right) = 0 \tag{A.2}$$

Note that the periodic function $\text{sign}(\cos(u))$ can be decomposed into the sum of simpler oscillating functions in terms of the Fourier series to reveal the contribution of each harmonic. Thus, it can be written that

$$\begin{aligned} \text{sign}(\cos(\omega t)) = &\ \textstyle\sum_{i=1,3,5,\cdots}^{\infty} A_i \cos(i\omega t) \\ = &\ A_1\cos(\omega t) + A_3\cos(3\omega t) + \cdots \end{aligned} \tag{A.3}$$

We will consider only the first two terms of this series as the higher-order elements can not be turned into resonant terms when multiplied by $(1+\cos(2\omega t))$. Following algebra manipulation the last term of Equation (A.2) can be expressed as

$$\begin{aligned} &(1+\cos(2\omega t))\text{sign}\left(\cos\left(\omega t\right)\right) \\ &\quad = \left(1+\cos\left(2\omega t\right)\right)\left(A_1\cos(\omega t) + A_3\cos(3\omega t) + \cdots\right) \\ &\quad = A_1\cos(\omega t) + \tfrac{A_1}{2}(\cos(\omega t)+\cos(3\omega t)) + \tfrac{A_3}{2}(\cos(\omega t)+\cos(5\omega t)) \\ &\qquad + A_3\cos(3\omega t) + \cdots \end{aligned} \tag{A.4}$$

Considering only the resonant terms and using the values found for the Fourier coefficients, $A_1 = \frac{4}{\pi}$ and $A_3 = -\frac{4}{3\pi}$, this simplifies to

$$\left(1+\cos\left(2\omega t\right)\right)\text{sign}\left(\cos\left(\omega t\right)\right) = \tfrac{1}{2}(3A_1 + A_3)\cos(\omega t) = \tfrac{16}{3\pi}\cos(\omega t) \tag{A.5}$$

After substituting this result into Equation (A.2), we obtain an expression that disregards the contribution of higher-harmonic terms

$$-\omega^2 U\cos(\omega t) + \omega_n^2 U\cos(\omega t) + \frac{8}{3\pi}kU^2\cos(\omega t) = 0 \tag{A.6}$$

This result shows that the quadratic nonlinearity of the form $u|u|$ contributes to the system response at the fundamental frequency and the backbone curve, which may be written as

$$\omega^2 = \omega_n^2 + \frac{8}{3\pi}kU \tag{A.7}$$

In addition, taking the first derivative of ω^2 with respect to U in Equation (A.7) and evaluating the resulting function when $U \to 0$, allow us to show that the quadratic term $u|u|$ also produces a non-infinite gradient in the backbone curve at zero amplitude of response.

$$\frac{\partial \omega^2}{\partial U}_{U=0} = \frac{8}{3\pi}k \tag{A.8}$$

Note that in contrast to $u|u|$, if u^2 is used such that $\ddot{u} + \omega_n^2 u + ku^2 = 0$, the equivalent to (A.4) may be written as $\cos^2(\omega t) = \frac{1}{2}(1 + \cos(2\omega t))$. Hence here there is no contribution to the resonant response and so the resonant expression for the backbone curve is unaffected by the u^2 nonlinearity.

Appendix B. Matrices for the numerical example structure

Using the geometry and material characteristics defined before in Section 3, the following Lagrange's equations are defined to derive the equation of motion of the undamped underlying linear system

$$\frac{d}{dt}\left(\frac{\partial L}{\partial \dot{\mathbf{q}}}\right) + \frac{\partial L}{\partial \mathbf{q}} = 0 \tag{B.1}$$

where the Lagrangian $L = T - V$; $\mathbf{q} = \{q_0,\ q_1,\ q_2,\ q_3,\ q_4,\ q_5,\ \theta_1,\ \theta_2\}^T$ and $(\dot{})$ indicates the first derivative with respect to time. Here T is the total kinetic energy of the system and V the potential energy of the system. For the example structure in Figure 2, these can be expressed as follows

$$\begin{aligned} T =& \frac{1}{2}\int_{-L}^{L} m\dot{y}^2 dz + \frac{1}{2}M\left(\dot{y}(t,-a)^2 + \dot{y}(t,a)^2\right) \\ &+ \frac{1}{2}Mb^2\left(\left(\dot{\theta}_1 + \frac{\partial y}{\partial z}(t,-a)\right)^2 + \left(\dot{\theta}_2 + \frac{\partial y}{\partial z}(t,a)\right)^2\right) \end{aligned} \tag{B.2}$$

$$\begin{aligned} V =& \frac{1}{2}EI\int_{-L}^{L}\left(\frac{\partial^2 y}{\partial z^2}\right)^2 dz + \frac{1}{2}k_s\left(y(t,-L)^2 + y(t,L)^2\right) \\ &+ Mgb\left(2 - \cos\left(\theta_1 + \frac{\partial y}{\partial z}(t,-a)\right) - \cos\left(\theta_2 + \frac{\partial y}{\partial z}(t,a)\right)\right) \end{aligned} \tag{B.3}$$

where m is the mass per unit of length along the beam, L is the length of the beam, M is the mass of the stores located a distance a from the beam's centre, g is the acceleration of gravity, EI is the flexural rigidity of the beam and b is the perpendicular distance from the store to the principal beam's axis. All the other parameters are defined in Section 3.

After substituting equations (B.2) and (B.3) into the Lagrangian L and calculating the derivatives indicated in (B.1), the following mass and stiffness matrices can be computed for the example structure

$$\mathbf{M} = \begin{bmatrix} 6.750 & 0 & 2.351 & 0 & 1.084 & 0 & 0 & 0 \\ 0 & 2.472 & 0 & 1.215 & 0 & 0.679 & 0.030 & 0.030 \\ 2.351 & 0 & 1.259 & 0 & 0.726 & 0 & -0.036 & 0.036 \\ 0 & 1.215 & 0 & 0.742 & 0 & 0.478 & 0.033 & 0.033 \\ 1.084 & 0 & 0.726 & 0 & 0.484 & 0 & -0.026 & 0.026 \\ 0 & 0.679 & 0 & 0.478 & 0 & 0.344 & 0.020 & 0.020 \\ 0 & 0.030 & -0.036 & 0.033 & -0.026 & 0.020 & 0.015 & 0 \\ 0 & 0.030 & 0.036 & 0.033 & 0.026 & 0.020 & 0 & 0.015 \end{bmatrix} \text{(Kg)} \quad \text{(B.4)}$$

$$\mathbf{K} = \begin{bmatrix} 0.020 & 0 & 0.020 & 0 & 0.020 & 0 & 0 & 0 \\ 0 & 0.021 & 0 & 0.021 & 0 & 0.021 & 0.0003 & 0.0003 \\ 0.020 & 0 & 1.048 & 0 & 2.075 & 0 & -0.0003 & 0.0003 \\ 0 & 0.021 & 0 & 3.101 & 0 & 6.181 & 0.0003 & 0.0003 \\ 0.020 & 0 & 2.075 & 0 & 7.413 & 0 & -0.0002 & 0.0002 \\ 0 & 0.021 & 0 & 6.181 & 0 & 14.687 & 0.000 & 0.000 \\ 0 & 0.0003 & -0.0003 & 0.0003 & -0.0002 & 0.0002 & 0.0196 & 0 \\ 0 & 0.0003 & 0.0003 & 0.0003 & 0.0002 & 0.0002 & 0 & 0.0196 \end{bmatrix} \times 10^4 \text{(N/m)} \quad \text{(B.5)}$$

We assume damping ratios of 0.5% of the critical damping in all modes and use the matrix of mode shapes presented in Appendix C to compute the damping matrix $\mathbf{C}$ as

$$\mathbf{C} = \begin{bmatrix} 3.658 & -0.000 & 1.355 & -0.000 & 0.657 & -0.000 & -0.003 & 0.003 \\ -0.000 & 2.283 & 0.000 & 1.148 & 0.000 & 0.656 & 0.029 & 0.029 \\ 1.355 & 0.000 & 6.000 & 0.000 & 5.605 & 0.000 & -0.232 & 0.232 \\ 0.000 & 1.148 & 0.000 & 5.315 & 0.000 & 6.355 & 0.161 & 0.161 \\ 0.657 & 0.000 & 5.605 & 0.000 & 9.099 & -0.000 & -0.155 & 0.155 \\ 0.000 & 0.656 & 0.000 & 6.355 & 0.000 & 9.376 & 0.077 & 0.077 \\ -0.003 & 0.029 & -0.232 & 0.161 & -0.155 & 0.077 & 0.165 & 0.001 \\ 0.003 & 0.029 & 0.232 & 0.161 & 0.155 & 0.077 & 0.001 & 0.165 \end{bmatrix} \times 10^{-1} \text{(Ns/m)} \quad \text{(B.6)}$$

Similarly, the force vector in Equation (2) can be computed as

$$\mathbf{F} = \left[\begin{array}{cccccccc} 1 & \frac{p}{L} & \left(\frac{p}{L}\right)^2 & \left(\frac{p}{L}\right)^3 & \left(\frac{p}{L}\right)^4 & \left(\frac{p}{L}\right)^5 & 0 & 0 \end{array} \right]^T \tag{B.7}$$

where p is the distance where the point force is applied, i.e., $L/3$.

In addition, the location vectors of the nonlinearities multiplied by the matrix of mode shapes can be written as

$$\rho_1\Phi = \left[\begin{array}{cccccccc} 0.0 & 0.001 & 3.61 & -5.48 & 6.55 & 5.45 & -1.23 & 8.81 \end{array} \right] \tag{B.8}$$

$$\rho_2\Phi = \left[\begin{array}{cccccccc} 0.0 & 0.001 & -3.61 & -5.48 & -6.55 & 5.45 & 1.23 & 8.81 \end{array} \right] \tag{B.9}$$

Appendix C. Mode shapes of the numerical example structure

The complete matrix of mode shapes for the example structure in Section 3 is as follows. Note that this matrix is normalised with respect to the mass matrix such that $\Phi^T M \Phi = I$; where I is the identity matrix.

$$\Phi = \left[\begin{array}{cccccccc} 0.387 & 0.000 & 0.266 & 0.000 & -0.688 & 0.000 & 0.683 & 0.000 \\ -0.000 & -0.638 & -0.000 & 0.298 & 0.000 & 1.919 & 0.000 & 3.807 \\ -0.007 & -0.000 & -0.862 & -0.000 & 2.187 & -0.000 & -4.542 & 0.000 \\ 0.000 & 0.006 & 0.000 & -0.426 & -0.000 & -5.177 & -0.000 & -16.232 \\ 0.001 & 0.000 & 0.190 & 0.000 & -0.458 & -0.000 & 5.600 & 0.000 \\ -0.000 & -0.002 & -0.000 & 0.165 & 0.000 & 1.785 & 0.000 & 14.389 \\ -0.000 & 0.001 & 3.609 & -5.475 & 6.546 & 5.453 & -1.234 & 8.810 \\ 0.000 & 0.001 & -3.609 & -5.475 & -6.546 & 5.453 & 1.234 & 8.810 \end{array} \right] \tag{C.1}$$